Physics Letters A 382 (2018) 1014–1019

Contents lists available at ScienceDirect

Physics Letters A

www.elsevier.com/locate/pla

Internal transport barriers in plasmas with reversed plasma flow

R.M. Ferro *, I.L. Caldas

Institute of Physics, University of São Paulo, São Paulo, SP, Brazil

ARTICLE INFO

Article history:
Received 15 November 2016
Received in revised form 26 August 2017
Accepted 14 February 2018
Available online 20 February 2018
Communicated by F. Porcelli

Keywords:
Transport barrier
Reversed plasma flow
Helimak

ABSTRACT

Evidences of internal particle transport barriers have been observed in plasma discharges with reversed plasma flow. To investigate the influence of the radial electric field profile on these barriers, we apply a drift wave map that describe the plasma particle transport and allows the integration of particle drift in the presence of a given electrostatic turbulence spectrum. With this procedure we show that transport barriers due to the shearless flow invariant lines are created inside the plasma. Moreover, by varying the radial electric field profile, we observe the formation and destruction of internal transport barriers constituted by shearless invariant lines, as well as its effects on the transport in the map's phase space. Applicability of our results are discussed for the Texas Helimak, a toroidal plasma device in which the radial electric field can be changed by application of bias potential.

1. Introduction

In fusion devices, as tokamaks and stellarators, plasma confinement is limited by the anomalous particle transport at the plasma edge driven by the electrostatic turbulence observed at this region [1]. Meanwhile, several experiments have shown that such turbulence and transport could be reduced by imposing an external electric potential that changes the radial electric field profile [2,3]. Furthermore, several experiments show that this transport can be reduced by properly changing the shear radial profile of the radial electric field component (the shear is proportional to the radial gradient of the field component) [3]. In this context, one experimental procedure to change the shear and reduce the transport is to apply a bias voltage to properly modify the radial electric field profile. On the other hand, the radial electric field and the toroidal magnetic field give rise to a poloidal plasma drift flow in the same direction of the drift waves propagation. The shear of this flow is essentially determined by the electric field shear. Thus, electrode biasing has been applied to verify the influence of the electric shear on the plasma transport and the formation of edge transport barriers [3].

To interpret particle transport at the tokamak plasma edge, non-integrable drift models with chaotic dynamics have been proposed for large aspect ratio tokamaks [4]. Following this approach, a model has been proposed to describe the transport by drift waves propagating in the plasma edge of tokamaks with equilibrium $\vec{E} \times \vec{B}$ poloidal flow, for uniform magnetic fields. Moreover, local symplectic drift wave maps have been derived from these models [4] to numerically investigate the transport dependence on shear spatial profiles. In particular, a non monotonic plasma equilibrium with reversed shear flow may generate a shearless invariant, in the radial position where the shear changes signal, acting as a transport barrier.

In this context, a model to describe drift wave test particle transport in reversed shear plasmas was considered to explain the reduction of turbulence-induced transport by the formation of shearless internal transport barriers in TCABR Tokamak (University of São Paulo, Brazil) [5] and Texas Helimak (University of Texas at Austin) [6].

To improve the experimental knowledge of turbulence and transport control, experiments have also been performed in devices confining plasmas with selected characteristics of a fusion plasma in a simpler geometry and with better diagnostics than those possible in major confinement devices. Thus, the external electric potential dependence of particle transport have been investigated in the Large Plasma Device (LAPD) [7], and in the helimaks BLAAMANN [8], TORPEX [9], and Texas Helimak [10].

In Texas Helimak a large set of diagnostic probes is used to measure average parameters and fluctuations, and an independent spectroscopic diagnostic of the plasma flow is used to evaluate plasma flow shear's influence on particle transport [10]. Moreover, some of the analyzed discharges present a reversed shear plasma flow and are especially adequate to investigate shearless transport barrier onset predicted to this kind of flow.

An important technique that allows the long-time integration of particle orbits is to replace the actual guiding-center orbits with those of a symplectic map derived for a large aspect ratio

* Corresponding author.
E-mail addresses: rafaelmf@if.usp.br (R.M. Ferro), ibere@if.usp.br (I.L. Caldas).

https://doi.org/10.1016/j.physleta.2018.02.019
0375-9601/

plasma configuration [4]. Individual orbits obtained from the map can differ qualitatively from those obtained from the differential equations, but statistically maps tend to give correct quantitative predictions [4]. Although the exact ion orbits can be followed by integrating differential equations, maps are preferred to follow orbits accurately for the long time required to transport analysis.

We apply a map that describes particle orbits in drift waves to investigate the dependence of transport upon radial electric field with shear. This map reveals that the improved confinement for the reversed shear profile arises from a change in the topology of electric field and the concomitant persistence of invariant curves in a layer in the vicinity of the point where the shear reverses, the shearless point. Away from the shearless point, the transport degrades to that given by a monotonic twist map. Near the shearless point, however, the map characterizing the motion is a nontwist map. Thus, the transport is substantially reduced for the reversed shear profile. We also show how these internal shearless transport barriers are created and change as the electric field radial profile is modified by the applied bias voltage. We give examples of the transport barriers dependence on the bias voltage showing that the barriers can be created or annihilated by small changes of this control parameter. Applicability of our results are discussed for the Texas Helimak.

In Section 2 we present basic information about the Texas Helimak discharges with reversed plasma flow and the symplectic map applied in Section 3 to predict the transport barriers and their dependence on the applied bias voltage. Conclusions are in Section 4.

2. Test particle simulations

2.1. Reversed flow plasmas

In Texas Helimak a plasma toroidal device generates a low density and temperature plasma with a sheared cylindrical slab [10]. The equipment disposes of a large set of diagnostic probes used to measure average parameters and fluctuations, as well as an independent spectroscopic diagnostic used to measure the plasma flow profiles [11]. Moreover, some Texas Helimak discharges present a reversed shear plasma flow [6], a condition which is especially adequate to investigate shearless transport barrier onset predicted to this kind of flow.

Texas Helimak consists of a toroidal vacuum vessel with rectangular cross section of height $H = 2.0$ m, internal radius $R_{int} = 1.0$ m and external radius $R_{ext} = 1.6$ m, as shown in Fig. 1a. The magnetic field has a toroidal component, B_φ, generated by a set of sixteen toroidal field coils, and a vertical field, B_z, generated by a set of three vertical field coils. The toroidal field has magnitude of order 0.1 T and the ratio B_z/B_φ can be adjusted with resistors added to the vertical coils, so that the magnitude of the vertical field can reach values up to 10% of B_φ. Its main characteristics vary only with the radial coordinate, in a good approximation to one-dimensional plasma experiments.

One of the main characteristics of the Texas Helimak is the possibility to control the electric field radial profile by imposing an external electric potential through a set of bias plates. There are sixteen bias plates distributed at the bottom and at the top of the vessel, and a set of them is connected to a bias voltage, while the others remain connected to the vessel ground (Fig. 1). Thus, with these plates, the unperturbed electric field radial profile can be modified by choosing the applied bias voltage fixed for each discharge. In particular, the data used as a reference for the present study were obtained from shots performed with positive bias voltages [12]. Studies on the effects of the bias potential indicate modifications on the power spectrum and turbulence of the plasma [11]. In Texas Helimak, a spectrometer is used for measuring the vertical velocity flow (V_z) profile of the plasma through

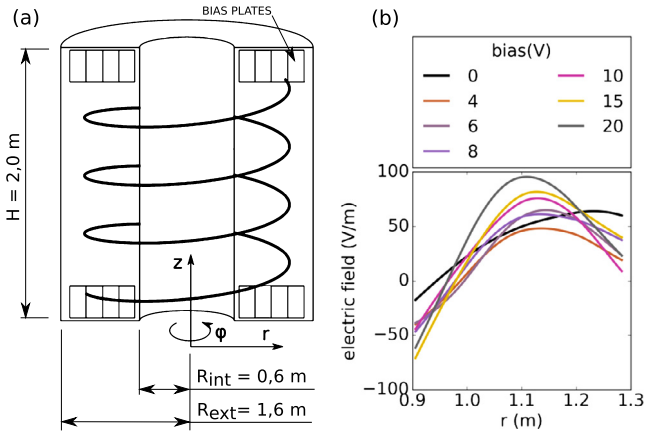

Fig. 1. (a) Schematic of the Texas Helimak and (b) plasma flow radial profile, for several applied positive bias voltage, in Texas Helimak [11,6]. (For interpretation of the colors in the figure(s), the reader is referred to the web version of this article.)

Doppler effect [11]. Fig. 1b shows the measured plasma flow radial profiles with reversed shear. These profiles will be considered in this work to predict the onset of shearless barriers.

For this study, data analyzed in previous works [6,12] at the Texas Helimak is used as a reference to calculate the parameters of the proposed drift wave map. For parameters similar to those observed in Texas Helimak discharges with positive bias, we investigate the shearless transport barriers dependence on the applied bias voltage. Our investigation, based on a map model introduced in the next section, allows to understand the origin of the shearless barriers instead of giving precise quantitative predictions of these barriers.

2.2. Drift wave map

We consider a model for drift wave maps [4] which assumes that the guiding center motion is governed by $\vec{E} \times \vec{B}$ drift. The equation of motion is then given by

$$\frac{d\vec{x}}{dt} = v_\parallel(t)\frac{\vec{B}}{B} + \frac{\vec{E}\times\vec{B}}{B^2} \tag{1}$$

The electric field is considered to have a radial mean part plus a fluctuating part

$$\vec{E} = E_0\hat{e}_r + \tilde{E}\,, \quad \tilde{E} = -\nabla\tilde{\phi} \tag{2}$$

where the perturbation electrostatic potential is given by the model drift wave spectrum

$$\begin{aligned}\tilde{\phi} &= \sum_{l,m,n}\phi_{l,m,n}\cos\left(m\varphi - l_z z - n\omega_0 t\right)\\ &= \sum_{l,m,n}\phi_{l,m,n}\left[\cos\left(m\varphi - l_z z\right)\cos\left(n\omega_0 t\right)\right.\\ &\quad \left. - \sin\left(m\varphi - l_z z\right)\sin\left(n\omega_0 t\right)\right]\\ &= 2\pi\sum_{l,m,n}\phi_{l,m,n}\cos\left(m\varphi - l_z z\right)\,\delta\left(\omega_0 t - 2\pi n\right)\end{aligned} \tag{3}$$

since

$$\sum_{n=-\infty}^{\infty}\cos\left(n\omega_0 t\right) = 2\pi\sum_{n=-\infty}^{\infty}\delta\left(\omega_0 t - 2\pi n\right) \qquad \text{and}$$

$$\sum_{n=-\infty}^{\infty}\sin\left(n\omega_0 t\right) = 0$$

with $l_z \equiv \frac{2\pi}{H} l$ $(l = 0, 1, \ldots)$ and $\phi_{l,m,n}$ are the waves amplitudes. The delta function argument introduced in the transformation contains the index n, which labels the time sequence of delta perturbations. Further approximations will be made for the amplitude and phase of the waves in the above equation.

A previous work [6] contains evidences that the $\vec{E} \times \vec{B}$ drift is sufficient to reproduce the alterations, observed in Texas Helimak discharges, of particle chaotic transport with the applied bias voltage and also the barriers radial position.

The physical motivation and justification for introducing a map in place of the differential equations follow from Texas Helimak plasma discharges perturbed by positive bias that show a wide frequency spectrum for a wave vector. We assume that for each drift wave vector there is a broad spectrum $n\omega_0$, $n = 1, 2, \ldots, N$ of frequencies. Here ω_0 is the lowest angular frequency with substantial amplitude in the drift wave spectrum. We idealize this spectrum by taking the limit $N \to \infty$ and assuming phase coherence of the components. It has been shown [4] that the result of these assumptions was to produce maps with the well-known $\vec{E} \times \vec{B}$ diffusivity induced by turbulent fluctuation. This albeit oversimplification of the drift wave spectrum captures the essential features of the $\vec{E} \times \vec{B}$ turbulent transport.

Once $B \approx B_\varphi \gg B_z$, the equation of motion gives

$$\frac{\mathrm{d}r}{\mathrm{d}t} = \frac{1}{B}\frac{\partial \tilde{\phi}}{\partial z} \tag{4}$$

$$r\frac{\mathrm{d}\varphi}{\mathrm{d}t} = v_\parallel \tag{5}$$

$$\frac{\mathrm{d}z}{\mathrm{d}t} = v_\parallel \frac{B_z}{B} + \frac{E_0}{B} - \frac{1}{B}\frac{\partial \tilde{\phi}}{\partial r} \tag{6}$$

The model assumes a dominant mode M/L with constant amplitude, so that the following change of variables is convenient

$$I = \frac{r^2 - R_{\mathrm{int}}^2}{R_{\mathrm{ext}}^2 - R_{\mathrm{int}}^2} \tag{7}$$

$$\chi = M\varphi - \frac{2\pi L}{H} z \tag{8}$$

The variable I is proportional to the area on the phase space and so is called the action variable, while χ has period 2π, being assigned to the angle variable. Applying this to Equation (4) gives the equation of motion in terms of action-angle variables. The perturbation term consists of periodic impulses on the action variable with period $T = 2\pi/\omega_0$. Thus the integration of the new equations of motion over one impulse results

$$I_{n+1} = I_n + \alpha \sin(\chi_n) \tag{9}$$

$$\chi_{n+1} = \chi_n + \frac{\beta}{\sqrt{I_{n+1} + b^2}} \tag{10}$$

where $b^2 \equiv R_{int}^2/(R_{ext}^2 - R_{int}^2)$, with parameters α and β related to physical variables by

$$\alpha \equiv \frac{2\pi}{\omega_0}\frac{2L\phi}{qa^2 B_z} \tag{11}$$

$$\beta \equiv \frac{2\pi}{\omega_0}\frac{1}{aq}\left[v_\parallel (Mq - L) - L\frac{E_0}{B_z}\right] \tag{12}$$

The map has two control parameters α and β which determine the orbit configuration in the phase space (I, χ). To obtain these parameters in the presented analysis investigating the influence of the electric field profile, we choose q and ϕ constants and a $E_0(I)$ profile.

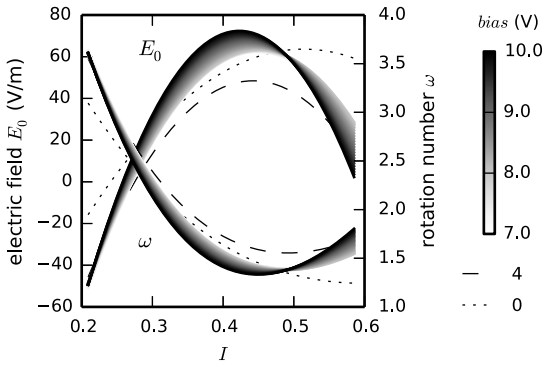

Fig. 2. Variation of the electric field radial profile and rotation number of the integrable map ($\alpha = 0$), with $\chi_0 = 0.5$, for various values of bias potential.

For a null perturbing amplitude wave, $\phi = 0$, Equation (11) implies $\alpha = 0$ and the map is integrable, namely, each trajectory is regular, either periodic or quasi-periodic, and stays in an invariant line with the initial action I_0 being a constant of motion. In this case, for each map iterate, the associated helical angle χ increases by a constant $\omega = \Delta\chi$, defined as the rotation number, which characterizes the invariant line. In general, for other α values we may have a mixed systems with chaotic trajectories and regular trajectories in invariant lines. In that sense, the rotation number profile can be an indicative of the behavior of the trajectories in any region of the phase space. For the non-integrable case we can still define a rotation number of an invariant line, considering an initial condition χ_0, as the limit

$$\omega(\chi_0) = \lim_{n\to\infty} \frac{\hat{\chi}_n - \hat{\chi}_0}{n} \tag{13}$$

where $\hat{\chi}_n$ refers to angle variable without modulo operator, that is mod $(\hat{\chi}_n, 2\pi) = \chi_n$, and n refers to the nth iteration. Fig. 2 shows the rotation number profile $\omega(\chi_0 = 0.5, I)$ for the non-perturbed map given by Equations (9)–(10). The local maximum/minimum (if it exists) of the rotation number profile $\omega(\chi_0)$ corresponds to the location of the shearless curve, which is an invariant line typical of non-twist systems.

Note that the rotation number depends on the control parameter β given by equation (12) and, therefore, on the electric field profiles $E_0(I)$. In the next section, we show the influence of the sheared electric field radial component, namely the profile $E_0(I)$ shown in Fig. 2, on the particle transport. In particular, we will look for the invariant lines with an extremum rotation number value which divide the phase space in two regions and acts as internal transport barriers.

3. Bias dependence of internal transport barriers

It has been shown in reference [6] (see Fig. 10 in this reference) that the experimental particle transport in Texas Helimak changes with the applied positive bias values. Moreover, for all applied bias values the particle transport is very small where the velocity shear is null. This observation was interpreted as an indication of a transport barrier localized in the plasma velocity (or electric field) shearless region. In this section we show, even for the simple model used, that shearless transport barriers are expected for a helimak with profiles like those observed in the Texas Helimak discharges analyzed in [9]. The predicted transport decrease is due to the non-monotonic vertical drift flow created by the radial electric field and the toroidal magnetic field.

In this section we consider the reference values to estimate the parameters of the drift wave map in Equations (9)–(10). The electric field profile $E_0(I)$ changes with the imposed bias voltage, the

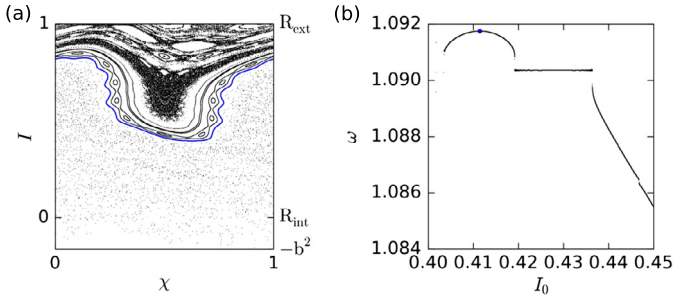

Fig. 3. *bias* = 0 V: (a) Phase space and (b) rotation number for initial conditions with $\chi_0 = 0.5$. In (a), the blue line indicates the shearless invariant curve; in (b), the blue dot indicates the local maximum of the rotation number profile, which corresponds to the location of the shearless curve in (a).

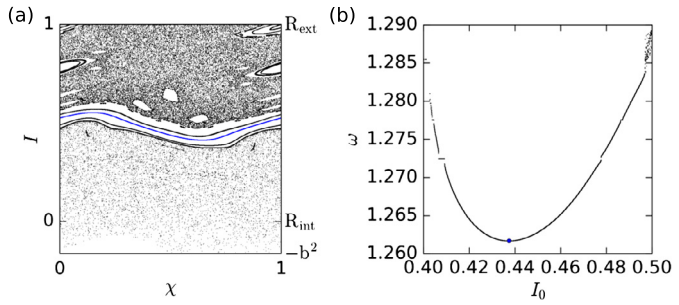

Fig. 4. *bias* = 4 V: (a) Phase space and (b) rotation number for initial conditions with $\chi_0 = 0.5$. In (a), the blue line indicates the shearless invariant curve; in (b), the blue dot indicates the local minimum of the rotation number profile, which corresponds to the location of the shearless curve in (a).

control parameter considered in our analysis. Fig. 2 illustrates how the electric field changes as the bias potential is increased from 0 to 10 V. It shows the bias potential values of 0 (dashed line) and 4 V (dash-dot line), as well as a continuous variation from 7 to 10 V. Each value of the bias potential represents one shot configuration in the device and defines an electric field profile $E_0(I)$. Hence, the parameter β of the map is estimated for each value of bias potential and is related to an electric field profile. The profiles shown in are obtained by interpolating profiles measured in Texas Helimak for bias potential of 0, 4, 6, 8, 10, 15 and 20 V. In Texas Helimak discharges with positive bias, the plasma flow profiles are non monotonic, as shown in Fig. 1b. The radial profiles shown in Fig. 2 are obtained by interpolating profiles of the radial electric field assuming that the velocity flow, measured in Texas Helimak for bias potential of 0, 4, 6, 8, 10, 15, 20 V [11,12], is equal to the electric drift velocity.

For the numerical estimations we use parameters chosen to represent the mentioned experiments with reversed shear flow in Texas Helimak. Accordingly, to iterate the map for the considered $E_0(I)$ profiles, we choose the constants $\phi = -10$ V, for the perturbation amplitude, $q = 2.89$ for the safety factor, and $M/L = 2/3$ for the dominant modes. The variables I, χ values were normalized to be between 0 and 1. We also consider the escape condition $\sqrt{I_{n+1} + b^2} \leq 0$, i.e. iterations are interrupted if $I \leq -b^2$. Thus, on the phase space graphs we indicate the values R_{ext}, R_{int} and $-b^2$ on vertical axis, and $\chi \to \chi/2\pi$ on horizontal axis.

Initially, to show the influence of the electric field profile on the particles confinement, we iterate the map Equations (9) and (10), for 0 and 4 V and a conveniently chosen set of 10×10 initial conditions and 500 iterates for each initial condition. The obtained phase space of Fig. 3 and Fig. 4 show internal barriers separating the particles in two phase space regions. From the rotation number profiles shown in Fig. 3b and Fig. 4b, calculated numerically for $\chi_0 = 0.5$ and sequences of 10^4 iterates, we can find the initial value of I_0 corresponding to the rotation number minimum or maximum. Iterating the initial conditions (I_0, χ_0) we obtain the shearless curves (blue line) of Fig. 3 and Fig. 4.

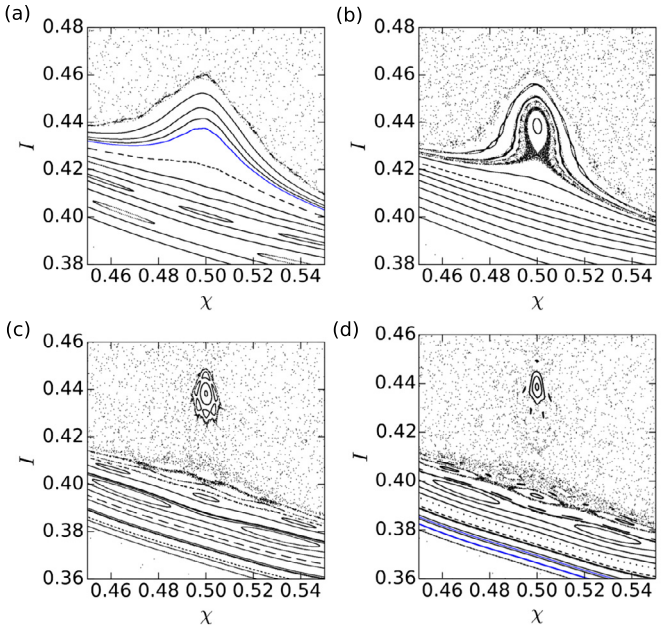

Fig. 5. Phase spaces for bias voltages (a) 7.8, (b) 7.9, (c) 8.4 and (d) 8.5 V. The blue lines in figures (a) and (d) indicate the shearless invariant curve.

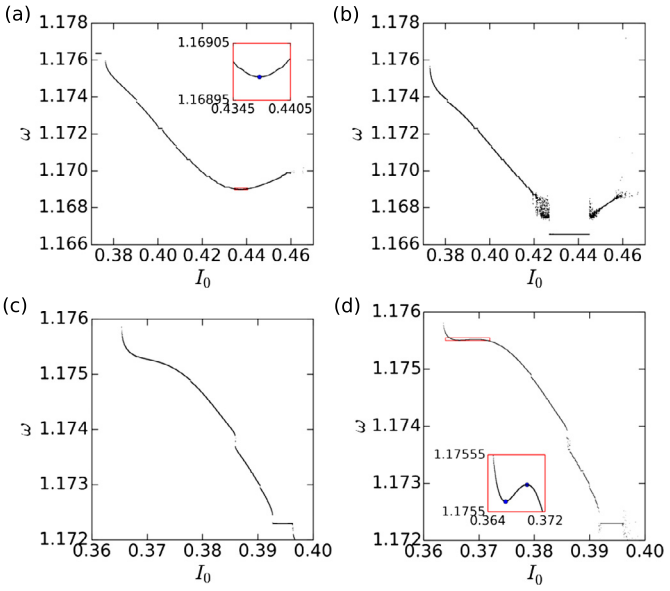

Fig. 6. Rotation number for bias voltages (a) 7.8, (b) 7.9, (c) 8.4 and (d) 8.5 V, calculated numerically for initial conditions with $\chi_0 = 0.5$. Details of figures (a) and (d) show the location of the shearless curve.

To show how sensitive the internal shearless transport barriers are to small control parameter change, we compare phase spaces obtained for a continuous variation of the $E_0(I)$ profile, show in Fig. 2, as the bias voltage changes from 7.0 to 10.0 V, obtained by interpolating the measured profiles for 6, 8 and 10 V.

In Fig. 5, we show the phase spaces obtained for 7.8, 7.9, 8.4, and 8.5 V. The shearless invariant line appears in the first and in the last of theses figures. From the corresponding rotation number profiles obtained for the surviving invariant lines, we see (Fig. 6) that the shearless line was annihilated and reappeared as the bias voltage increases.

In Fig. 6a, we see that the location of the shearless curve corresponds to a minimum of the rotation number profile. In fact, as the bias voltage increases from 4 to 7.8 V, the rotation number profile exhibits a minimum. For bias voltage of 7.9 V, the region of the phase space where once there were invariant curves gives rise to islands and chaotic subsets (Fig. 5b). The rotation number profile for this value of bias (Fig. 6b) shows a plateau in that region, which was the location of the minimum in Fig. 6a.

On the other hand, as the bias voltage is increased from 7.9 V, the islands formed near the shearless curve moves away from it (Fig. 5c) and the rotation number profile tends to bend and reverse its concavity (Fig. 6c). Then a minimum and a maximum appear at value 8.5 V, as seen in Fig. 6d. These points indicate the rising of other shearless curves (Fig. 6d) for values of I lower than those on the previous cases. Further increase on the bias voltage leads to the destruction of the shearless curves. For 8.7 V bias voltage, one curve disappears, and for 10 V, the remaining curve fades and the chaotic orbits may spread through the whole phase space.

As we see in Fig. 5c and Fig. 6d, the variation of the electric field profile and, consequently, the variation of the parameter β as a function of the action coordinate modifies the map in such a way that the rotation number does not exhibit an extremum. Although all the maps of Fig. 5c still preserve invariant curves that may separate trajectories in the phase space, not all of them produce the shearless curve, which is a characteristic of the non-twist systems. As expected, the surviving invariant curves are not so robust as the shearless curves and could be easily broken by changing the wave amplitude [13]. In other words, the transition to global chaos is affected by the presence of the shearless curve [13], thus its presence should reduces the transport in Texas Helimak.

3.1. Chaotic transport

To analyze the bias influence on the chaotic particle transport in configurations with no remaining transport barriers, we consider an ensemble of N chaotic particles randomly distributed in a specified domain of phase space. For each particle we consider that an initial state (I_0, χ_0) evolves to a final state (I_n, χ_n) at step n. Because of the spatial periodicity of the waves, an average over this region is equivalent to an average over the entire accessible phase space. The radial coordinate of particle i (determined by its action) is r_i and the initial radial position is $r_i(0)$. Thus, we calculate the quadratic deviation of a particle's trajectory for each initial radial position, for $N = 10000$ initial conditions evenly distributed in the region $0.4 \leq \chi \leq 0.6$, $0.9 \leq I \leq 1$. The particle average quadratic deviation, σ, of the radial drift excursions in the chaotic region can be defined as

$$\sigma(n) = \sqrt{\frac{1}{N}\sum_{i}^{N}(r_i(n) - r_i(0))^2} \tag{14}$$

Thus, calculating the presented quadratic deviation for a set of initial conditions we can follow the trajectories and estimate the forward particle displacement until they escape the plasma [14, 15]. This procedure is an alternative to the use of the trajectory standard deviation, adequate to analyze deviations from average values.

In Fig. 7a, we see that the average quadratic deviation of the radial position tends to increase for higher values of the bias voltage, as the remaining trajectories decrease. However, we see that, for high n values, the transport is not diffusive, i.e., σ^2 does not increase linearly with n. Therefore, in this case, we can not define the coefficient of diffusion as the limit of $\sigma^2/2n$ for n going to infinite.

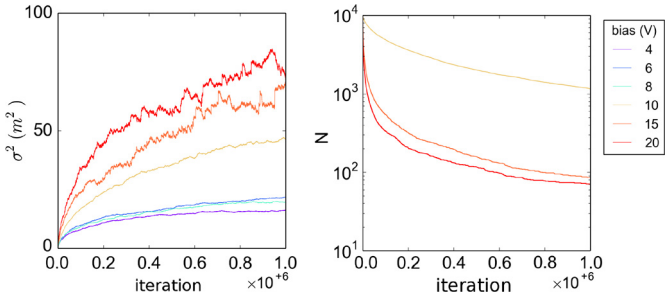

Fig. 7. (a) Standard deviation for particle radial position and (b) remaining trajectories over time for some values of bias voltage.

For the same set of the mentioned initial conditions, we plot the quantity of remaining trajectories over iteration time for values of bias that no longer preserve the barrier.

Thus, after the shearless barriers are broken, the transport increases with the applied bias voltage, as expected by the destruction of invariants lines and islands as the bias increases. Therefore, the considered drift wave map allows understanding how the chaotic radial particle transport develops as the bias voltage increases.

4. Conclusions

We investigated the particle transport dependence on the electric field radial profile in sheared flow plasma discharges. For our predictions, we applied a drift wave map previously proposed to the integration of orbits on the long transport time scales, which is practically impossible for the differential equations governing the exact guiding-center orbits. Calculations using this map showed that a shearless flow transport barriers can occur for reversed shear flow profiles. Furthermore, we show that the shearless transport barriers change as the electric field radial profile is modified by the applied bias voltage. These transport barriers are sensitive to the bias voltage and can be created or annihilated by small changes of this control parameter.

The numerical results, obtained for the Texas Helimak parameters in discharges with positive applied bias voltage, support previous reported evidences of shearless transport barriers and allow us to predict the onset and annihilation of internal transport barriers in this device as the bias voltage is modified.

Furthermore, the procedure introduced in this article could be extended for modified electric field profiles due to finite Larmor radius [16] or due to displaced resonances predicted for plasmas with energetic particles [17].

Acknowledgements

The authors thank the financial support from the Brazilian Federal Agencies CNPq and CAPES, and the São Paulo Research Foundation (FAPESP, Brazil) under grant No. 2011/19296-1. The authors also acknowledge discussions with Profs. K. Gentle and P. J. Morrison from the University of Texas at Austin (USA), Drs. Z. O. Guimarães and F. A. Pereira from the University of São Paulo, and D. L. Toufen from Federal Institute of Education, Science and Technology of São Paulo.

References

[1] W. Horton, Drift waves and transport, Rev. Mod. Phys. 71 (3) (1999) 735.
[2] C. Hidalgo, On the nature of transport in fusion plasmas, Astrophys. Space Sci. 292 (2004) 681.
[3] G.V. Oost, J. Adamek, V. Antoni, P. Balan, J.A. Boedo, P. Devynck, I. Duran, L. Eliseev, J.P. Gunn, M. Hron, C. Ionita, S. Jachmich, G.S. Kirnev, E. Martines, A. Melnikov, R. Schrittwieser, C. Silva, J. Stockel, M. Tendler, C. Varandas, M.V.

Schoor, V. Vershkov, R.R. Weynants, Turbulent transport reduction by e x b velocity shear during edge plasma biasing: recent experimental results, Plasma Phys. Control. Fusion 45 (5) (2003) 621.
[4] W. Horton, P. Hyoung-Bin, K. Jae-Min, D. Strozzi, P.J. Morrison, C. Duk-In, Drift wave test particle transport in reversed shear profile, Phys. Plasmas 5 (11) (1998) 3910.
[5] F.A. Marcus, I.L. Caldas, Z.d.O. Guimarães-Filho, P.J. Morrison, W. Horton, Y.K. Kuznetsov, I.C. Nascimento, Reduction of chaotic particle transport driven by drift waves in sheared flows, Phys. Plasmas 15 (11) (2008) 112304.
[6] D.L. Toufen, Z.d.O. Guimarães-Filho, I.L. Caldas, F.A. Marcus, K.W. Gentle, Turbulence driven particle transport in Texas Helimak, Phys. Plasmas 19 (1) (2012) 012307.
[7] W. Gekelman, H. Pfister, Z. Lucky, J. Bamber, D. Leneman, J. Maggs, Design, construction, and properties of the large plasma research device – the LAPD at UCLA, Rev. Sci. Instrum. 62 (12) (1991) 2875.
[8] K. Rypdal, E. Gronvoll, F. Oynes, A. Fredriksen, R.J. Armstrong, J. Trulsen, H.L. Pécseli, Confinement and turbulent transport in a plasma torus with no rotational transform, Plasma Phys. Control. Fusion 36 (7) (1994) 1099.
[9] A. Fasoli, B. Labit, M. McGrath, S.H. Müller, G. Plyushchev, M. Podestà, F.M. Poli, Electrostatic turbulence and transport in a simple magnetized plasma, Phys. Plasmas 13 (5) (2006) 055902.
[10] K.W. Gentle, H. Huang, Texas Helimak, Plasma Sci. Technol. 10 (3) (2008) 284.
[11] K.W. Gentle, K. Liao, K. Lee, W.L. Rowan, Comparison of velocity shear with turbulence reduction driven by biasing in a simple cylindrical slab plasma, Plasma Sci. Technol. 12 (2010) 391.
[12] D.L. Toufen, Controle da turbulência em plasmas, Ph.D. thesis, Institute of Physics, University of São Paulo, 2012, http://www.teses.usp.br/teses/disponiveis/43/43134/tde-26032013-154737/publico/TOUFENDLtesedoutorado.pdf.
[13] D. del Castillo-Negrete, J.M. Greene, P.J. Morrison, Area preserving non-twist maps: periodic orbits and transition to chaos, Physica D 91 (1996) 1.
[14] A. Rechester, R.B. White, Calculation of turbulent diffusion for the Chirikov–Taylor model, Phys. Rev. Lett. 44 (24) (1980) 1586.
[15] A.N. Lichtenberg, M.A. Lieberman, Symplectic Maps, Variational Principles, and Transport, 2nd edition, Springer-Verlag, Berlin, 1992, Ch. 5, Eq. 5.33.
[16] J. da Fonseca, D. del Castillo-Negrete, I. Caldas, Area-preserving maps models of gyroaveraged $e \times b$ chaotic transport, Phys. Plasmas 21 (9) (2014) 092310.
[17] S. Ogawa, X. Leoncini, G. Dif-Pradalier, X. Garbet, Study on the creation and destruction of transport barriers via the effective safety factors for energetic particles, Phys. Plasmas 23 (12) (2016) 122510.